Investigation of the low-spin to high-spin transition in a novel [Fe(pmea)(NCS)2] complex by IR and Raman spectroscopy and DFT calculations

7 AUTHORS, INCLUDING:

Markus Reiher
ETH Zurich
289 PUBLICATIONS **8,532** CITATIONS

Boris Le Guennic
Université de Rennes 1
137 PUBLICATIONS **2,368** CITATIONS

Frank W. Heinemann
Friedrich-Alexander-University of Erlangen-…
498 PUBLICATIONS **6,096** CITATIONS

JRS

Investigation of the low-spin to high-spin transition in a novel [Fe(pmea)(NCS)₂] complex by IR and Raman spectroscopy and DFT calculations†

Georg Brehm,[1]* Markus Reiher,[2] Boris Le Guennic,[2] Michael Leibold,[4] Siegfried Schindler,[3] Frank W. Heinemann[4] and Siegfried Schneider[1]

[1] Institut für Physikalische und Theoretische Chemie, Universität Erlangen-Nürnberg, Egerlandstr. 3, D-91058 Erlangen, Germany

[2] Institut für Physikalische Chemie, Universität Jena, Helmholtzweg 4, 07743 Jena, Germany

[3] Institut für Anorganische und Analytische Chemie, Justus-Liebig-Universität Giessen, Heinrich-Buff-Ring 58, 35392 Gießen, Germany

[4] Institut für Anorganische Chemie, Universität Erlangen-Nürnberg, Egerlandstr.1, D-91058 Erlangen, Germany

The X-ray structures of the novel spin crossover complex [Fe(pmea)(NCS)₂] with pmea = (bis[(2-pyridyl)methyl]-2-(2-pyridyl)ethylamin) were determined in its low-spin (singlet, LS) and high-spin state (quintet, HS) and compared with the optimized geometries produced by BP86 calculations. IR and Raman (λ_{ex} = 514.5, 785 and 1064 nm) spectra were recorded at different temperatures between T = 298 K and T = 30 K. Most of the experimentally observed bands could be assigned unambiguously and discussed by comparison with the normal modes calculated for both spin states.

The detailed analysis of the temperature dependence of the band contours of specific modes provides strong evidence that significant changes of the inter-molecular distances occur for all molecules when a certain fraction of the individual molecules has undergone the low-spin (LS) to high-spin (HS) transition.

The partition function for intra-molecular vibrations was calculated for both spin states by considering all vibrational wavenumbers that were calculated. The vibration-related entropy change connected with the LS to HS transition is determined via well-established thermodynamic relations. For the title compound we found $\Delta S_{vib} \approx 40.3$ J/(mol·K), which is about twice that determined for [Fe(phen)₂(NCS)₂]. Consequently, the sum of the purely electronic contribution ($\sim$13.4 J/(mol·K)) and that of the intra-molecular vibrations equals the average entropic driving force determined for a series of spin-crossover complexes ($\sim$50 J/(mol·K)). It is therefore most interesting to experimentally determine the entropy change for the complex investigated here and to find out whether this complex exhibits an unusually large entropy change upon the LS to HS transition. Copyright © 2006 John Wiley & Sons, Ltd.

INTRODUCTION

Since its first discovery some 70 years ago,[1,2] the phenomenon of a thermally induced transition from a low-spin (LS) state predominant at low temperatures to a high-spin (HS) state at higher temperatures, usually termed as *thermal*

---

†**Presented as part of a commemorative issue for Wolfgang Kiefer on the occasion of his 65th birthday.**

*Correspondence to: Georg Brehm, Institut für Physikalische und Theoretische Chemie, Universität Erlangen-Nürnberg, Egerlandstr. 3, D-91058 Erlangen, Germany.
E-mail: georg.brehm@chemie.uni-erlangen.de

spin-crossover, has been extensively studied by a multitude of experimental techniques (for reviews see Refs 3–7). The high interest arose mainly for two reasons. One was the desire to understand this phenomenon on the basis of first principles, given the structure of the individual molecules and their arrangement in the crystal (specific and non-specific interactions).[6] The second driving force was its potential in a large variety of applications (displays, pressure and thermal sensors, detection of specific analytes like water).[7]

Generally, the transition from the LS to the HS state is considered to be driven by the increase in molar entropy ΔS, which amounts to about 50 J/(mol·K) in many examples,[8–11] but only about 13.4 J/(mol·K) originate from the electronic contribution, ΔS_{el}, if one deals with a transition from a singlet

to a quintet state (this is the case in most of the complexes containing iron as centre metal). According to Sorai and Seki,[8,9] a large contribution to ΔS can be expected because of the observed changes of the vibrational wavenumbers (ΔS_{vib}), and here mainly from the low-wavenumber modes related to the relative movement of the central metal ion and the (nitrogen) atoms that mediate the binding of the ligands.

To verify the above described conclusions, Bousseksou et al.[12] performed Raman experiments on [Fe(phen)$_2$(NCS)$_2$] at 300 K and 100 K in order to obtain the wavenumber shifts associated with the HS to LS transition. Rather than making the attempt to calculate the partition functions in both spin states, they determined an average wavenumber shift from the bands observed in the range below 500 and 600 cm^{-1}, respectively, and assumed this value to be representative for all 15 distortion modes of an idealized FeN$_6$ octahedron. According to Bousseksou et al.[12] the outcome of their first tentative approach 'seems reasonable despite the severe limitations of their procedure and illustrates the utility of Raman spectroscopy to assess the vibrational contribution to the entropy change associated with spin crossover.' Later, Brehm et al.[13] and Reiher et al.[14] re-investigated this system employing IR and Raman spectroscopy in combination with extensive DFT calculations. The partition function was determined for both spin states by considering all vibrational wavenumbers that were calculated. The vibration-related entropy change connected with the LS to HS transition resulted in $\Delta S_{vib} \approx 19.5$ J/(mol·K) thus verifying the estimate made by Bousseksou et al.[12]

In this contribution, we present IR and Raman spectra recorded at high and low temperature, respectively, of the novel spin-crossover complex [Fe(pmea)(NCS)$_2$]. This allows us to establish a large set of experimental wavenumbers, especially in the low wavenumber region and to validate the results of DFT calculations. On the basis of the complete set of calculated normal mode wavenumbers, we can calculate the contribution ΔS_{vib}.

MATERIALS AND METHODS

Materials

The synthesis and crystallographic characterization of the title compound [Fe(pmea)(NCS)$_2$] (for chemical structure see Scheme 1) is described in detail elsewhere.[15,16] [Fe(pmea)(NCS)$_2$] is closely related to [Fe(tmpa)(NCS)$_2$] and [Fe(DPEA)(NCS)$_2$], two complexes that have been described previously.[17,18]

A microcrystalline sample powder was used either directly or diluted in CsI (FIR) and KBr (MIR, Raman), respectively, and formed into a pellet. The employed concentration was usually about 20 mg sample/200 mg KBr matrix. The major reason for the latter procedure was that application of neat crystalline material resulted in immediate destruction, when the probing Raman laser (514.5
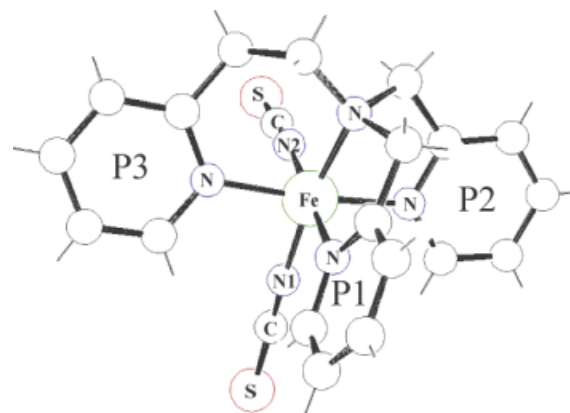
Scheme 1. Chemical structure of [Fe(pmea)(NCS)$_2$] and numbering of elements employed.

or 785 nm) was focused onto the sample. For FT-NIR Raman measurements, a neat sample powder was used.

IR and Raman spectroscopy

IR spectra of pellets with 5 mg sample/200 mg matrix were recorded on a Bruker Equinox 55 spectrometer (resolution 2 cm^{-1} in FIR and 1 cm^{-1} in MIR).

Raman spectra with 1064 nm excitation were recorded with a Bruker RFS100 FT-Raman spectrometer (I = 25 mW, $\phi \sim 1$ mm). Raman spectra with 785 nm excitation (I = 300 mW, $\phi \sim 0, 1$ mm) were collected employing a home-built Ti:Sapphire laser pumped by an Ar$^+$ laser (Coherent, Innova 90-6). After dispersion in a double grating spectrograph (Spex, model 1402), the Raman scattered light was detected by a liquid nitrogen-cooled CCD camera (ISA, model Spectrum One) with a spectral resolution of 2 cm^{-1}. The wavenumber reading of the dispersive Raman apparatus may differ by up to 4 cm^{-1} from that of the NIR-FT Raman spectrometer.

For recording spectra at low temperature, the sample was mounted on the cold finger of a closed-cycle refrigerator (CTI Cryogenics, model CCS-150) employing KBr (IR) and quartz windows (Raman), respectively, in the evacuated sample chamber. Since the temperature sensor was mounted on the sample holder, the temperature readings may not correspond precisely to the temperature of the probed sample region. Because consecutive measurements were performed upon cooling the sample, the actual temperature of the probed volume could be higher than the quoted temperature setting.

Quantum-chemical methodology

All calculations were performed with the density functional programs provided by the Turbomole 5.1 suite.[19] The Becke–Perdew functional (BP86[20,21]) was used in combination with the resolution of the identity (RI) technique.[22,23] Two different basis sets (Ahlrichs' TZVP[24] and the TZVPP basis set with TZV kernel plus Dunning polarization functions as implemented in Turbomole) were employed to

investigate the influence of their size on the results, especially ΔS_{vib}. The vibrational contribution to the total entropy was computed within the harmonic approximation of the force field using the analytical results for the partition function of a harmonic oscillator.[25] (More details on the applied programs can be found in our already cited previous publications.[13,14])

We chose the BP86 density functional as it is known to produce harmonic vibrational wavenumbers in good agreement with the measured fundamental ones[26,27] owing to an error compensation, which appears to be valid even for low-wavenumber modes.[14] Note, however, that the electronic energy difference between low- and high-spin state is difficult to obtain in DFT calculations and reparameterized hybrid density functionals should be used,[28] which turn out to be useful even for the most critical thermal spin-crossover complexes.[29]

The calculated normal coordinates were analysed with the help of the program 'Molden' provided by the Centre for Molecular and Biomolecular Informatics, Radboud University, Nijmegen, Netherlands.[30] Since a good graphic presentation of most of the normal coordinates is impossible, the input data for the program 'Molden' can be provided upon request to interested readers.

RESULTS

Structures and quantum-chemical calculations

For the lowest electronic state with singlet character, the BP86/RI/TZVPP calculations produce three energetically close-lying isomers. One of these matches closely with the low temperature X-ray structure of [Fe(pmea)(NCS)$_2$] (Fig. 1) and is therefore selected for the comparison between experimental and theoretical results. The complex exhibits C_1-symmetry with the two NCS-ligands in a cisoid arrangement. One of the NCS groups is found in an axial position (N1CS), the second axial position is occupied by the amino nitrogen, N(amino). The three remaining equatorial positions are occupied by the two pyridines (P1 and P2) that are connected to N(amino) via a CH$_2$ group, in a cisoid arrangement and by the third pyridine (P3) that is connected to N(amino) via a (CH$_2$)$_2$ link. The pyridines P1 and P3 are
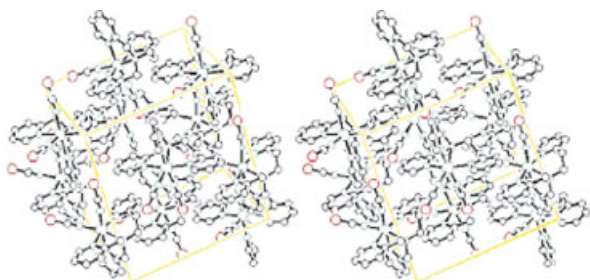

Figure 1. Stereo view of the X-ray structure of [Fe(pmea)(NCS)$_2$] in the low-spin state constructed with the program ORTEP III.[31]

nearly coplanar, whereas the plane of P2 is rotated by about 90° (Scheme 1 for numbering).

The optimized HS state (quintet) of the corresponding isotopomer matches the X-ray structure of [Fe(pmea)(NCS)$_2$] recorded at high (room) temperature. An overlay of the structures calculated for both spin states is shown in Fig. 2. It can be seen that the LS state structure (in red/dark grey) has smaller Fe–N distances than the HS state structure (in blue/light grey). The calculated and experimentally determined distances between the central iron and the six ligating nitrogen atoms are compared in Table 1. The expected increase in length of all metal-to-ligand bonds is reproduced by the calculations. The increase in bond length to the pyridine nitrogens N(P1) and N(P2) and to the amino nitrogen N(amino) is, however, overestimated by about 50%, whereas the increase of the bond length to the axial (NCS) ligand, (N1CS), is underestimated by about 50% (*vs* crystal structure). The change of the N=C bond lengths in the (NCS) ligands is relatively small in contrast with the significant observed wavenumber changes of the (N=CS) stretching vibrations.

For both geometries, the calculations yield a complete set of (real) normal mode wavenumbers. In accordance with our previous experience[14] we find that the wavenumbers of those modes, which comprise mainly 'in-plane' motions, depend only weakly on the size of the basis set used. The wavenumbers of those modes, which represent essentially 'out-of-plane' motions, change significantly. With respect to the calculation of ΔS_{vib} it is worth noting that the extended basis set (TZVPP) leads mostly to decreased wavenumbers for the LS complex and increased wavenumbers for the
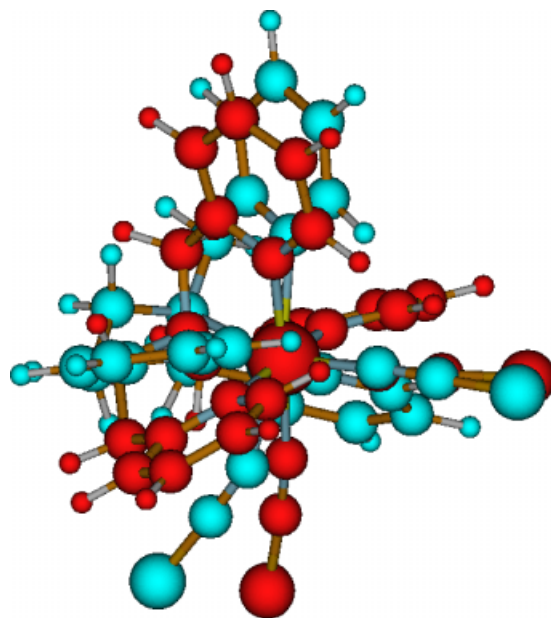

Figure 2. Overlay of the calculated structures of [Fe(pmea)(NCS)$_2$] in the low-spin and high-spin state, respectively. (BP86/RI/TZVPP calculations).

HS complex when only the vibrations below $100\,\mathrm{cm}^{-1}$ are considered (Table 3).

Very helpful for the intended correlation with the experimentally observed bands is that the produced wavenumbers can be grouped into blocks that are separated from each other by more than about $20\,\mathrm{cm}^{-1}$. The description given of the normal coordinates in Table 3 is based on visual inspection employing the program 'Molden' and refers, in case of large delocalization, to the (group) motions with the largest amplitudes.

Because the unit cell contains four molecules and exhibits C_{2v} symmetry, some selection rules may apply to the spectra recorded from crystalline material. Noteworthy is, the change of the dimensions of the unit cell on the LS to HS transition (Table 2). The relative increase is largest along direction **b** (3.4%) (the four axial ligating nitrogen atoms describe approximately the **bc** plane). The smallest increase is found along direction **a** (1.7%), which roughly coincides with the orientation of the equatorial NCS ligand. Consequently, the interaction between the various parts of the complex with neighbouring molecules will change in a different extent upon the LS to HS transition.

IR and Raman spectra

The transition temperature of [Fe(pmea)(NCS)$_2$] could be estimated by Moessbauer spectroscopy as $T_c = 190\,\mathrm{K}$.[15] Therefore, the IR and Raman spectra recorded at 300 K and 100 K respectively (Fig. 3) characterize well the HS (300 K) and LS complexes (100 K). In Table 3, the experimentally determined wavenumbers are summarized for comparison

Table 1. Comparison of selected geometrical parameters (bond lengths in pm) of [Fe(pmea)(NCS)$_2$] in the low-spin (LS) and high-spin (HS) state. (BP86/RI/TZVPP calculations)

Parameter	LS/ calc	LS/ exp	HS/ calc	HS/ exp	Δ/ calc	Δ/ exp
D [Fe−N1(CS)] (axial)	190.9	193.3	196.7	207.5	5.8	14.2
D [Fe−N2(CS)]	192.6	196.6	204.3	211.5	11.7	14.9
D [Fe−N(amino)] (axial)	206.3	204.4	239.5	226.2	33.2	21.8
D [Fe−N(P1)]	195.0	197.5	225.3	220.8	30.3	23.3
D [Fe−N(P2)]	197.0	199.1	220.8	219.7	23.8	20.6
D [Fe−N(P3)]	201.0	200.5	221.0	217.9	20.0	17.4
D [N1−(CS)] (axial)	119.1	116.6	119.7	114.6	0.6	−2.0
D [N2−(CS)]	118.8	116.9	119.2	114.5	0.4	−2.4

Table 2. Comparison of the dimensions of the unit cell of [Fe(pmea)(NCS)$_2$] in the low- and high-spin state

	Low-spin	High-spin	Increase (%)
Length **a**	14.989	15.242	1.7
Length **b**	10.438	10.820	3.4
Length **c**	13.341	13.699	2.6
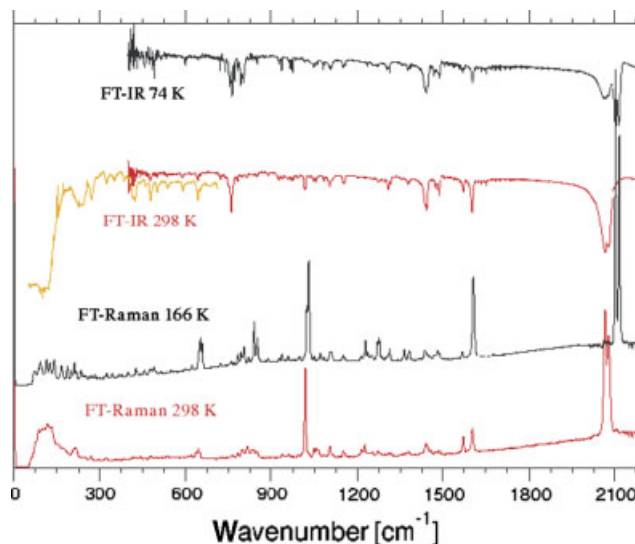
Figure 3. IR and Raman spectra ($\lambda_{ex} = 1064$ nm) of [Fe(pmea)(NCS)$_2$] recorded at 298 K (high-spin state) and 166 K/74 K (low-spin state). Spectral resolutions are $2\,\mathrm{cm}^{-1}$, FT-IR and $2\,\mathrm{cm}^{-1}$, FT-NIR Raman.

with the corresponding calculated ones. (Since the IR spectra recorded at low temperature obviously contain contributions from both the LS and HS complex we listed only the wavenumbers for the HS complex in Table 3. The tentative explanation is that the whole sample was not equilibrated at the present temperature.)

As discussed earlier,[3,34] in the FIR region ($100–500\,\mathrm{cm}^{-1}$) significant shifts of the ligand-central Fe(II) stretching vibrations are expected. One reason is that, upon transition to the HS state (in an ideal octahedral environment), an electron is promoted from a bonding t_{2g} orbital into an antibonding e_g orbital thus weakening the metal-to-ligand binding. On the other hand, the extent of $d_\pi - p_\pi$ back bonding to the ligand(s) is also reduced. If NCS groups are present as ligands the wavenumber of the antisymmetric and symmetric (N≡CS) stretching vibrations are lower in the HS state than in the LS state ($2065/2076\,\mathrm{cm}^{-1}$ *vs* $2104/2117\,\mathrm{cm}^{-1}$). The latter bands can conveniently be used as marker bands for the LS to HS transition because they are very well isolated in the spectra.

The Raman spectrum of the ligand pmea is dominated by a series of bands related to pyridine vibrations (Fig. 4): CH-stretch ($3054\,\mathrm{cm}^{-1}$), C=C-stretch (1583 and $1572\,\mathrm{cm}^{-1}$), ring deformation (C−C−C trigonal bending) and breathing (1010 and $992\,\mathrm{cm}^{-1}$), CH-i.p. bending ($1230\,\mathrm{cm}^{-1}$) and ring deformation (C−C−C i.p. bending, $605\,\mathrm{cm}^{-1}$). One can therefore expect several bands, related to these vibrations, to appear in the spectra of [Fe(pmea)(NCS)$_2$] eventually shifted because of the interaction with the central metal ion. If $d_\pi - p_\pi$ back bonding occurs also with the pyridine ligands then the bands related to the motion of the pyridine skeleton should, in addition, exhibit a detectable shift upon the LS

Table 3. Listing of calculated and experimental wavenumbers ($\tilde{v}$/cm^{-1}) of [Fe(pmea)(NCS)$_2$] in the low-spin (LS) and high-spin (HS) state. (Employed techniques: BP86/RI/TZVP and BP86/RI/TZVPP). Nomenclature applied in the assignment according to Wilson *et al.*[32] and Varsanyi,[33] respectively. (The Molden-files for depiction of the vibrations can be requested by e-mail)

| | Low-spin state | | | | High-spin state | | | | |
| | Calculated wavenumber (cm^{-1}) | | | Experimental (cm^{-1}) | Calculated wavenumber (cm^{-1}) | | | Experimental (cm^{-1}) | |
Mode no.	TZVP	TZVPP	Assignment	Raman	TZVP	TZVPP	Assignment	Raman	FT-IR
1	14.2	18.1	–	–	20.8	16.6	–	–	–
2	17.8	19.7	–	–	26.7	21.6	–	–	–
3	22.5	22.0	–	–	31.0	24.7	–	–	–
4	23.8	27.1	–	69	34.5	30.6	–	–	–
5	42.1	41.2	–	74	37.7	33.7	–	–	–
6	43.0	42.3	–	85	45.9	46.5	–	–	–
7	76.6	77.8	–	**91**	74.1	70.9	–	–	–
8	98.4	99.3	–	95	77.8	74.5	–	–	–
9	106.8	107.2	–	**113**	86.2	80.3	–	85	–
10	116.0	116.5	–	125	99.6	99.5	–	–	–
11	126.6	127.2	–	**140**	109.7	107.6	–	102	–
12	175.9	176.5	–	**165**	118.4	116.0	–	117	–
13	195.2	195.9	–	**185**	126.1	123.9	–	–	–
14	201.8	201.9	–	200	133.9	134.8	–	131	–
15	211.9	212.3	–	**210**	144.9	143.2	–	–	–
16	222.2	222.9	–	217	161.1	158.4	–	153	–
17	231.3	231.4	–	233	167.2	168.4	–	174	–
18	233.6	235.7	–	243	184.4	181.1	–	–	–
19	242.3	242.0	–	249	191.7	190.3	–	–	–
20	250.7	251.3	–	263	197.1	195.0	–	–	–
21	258.4	259.6	–	273	211.2	207.7	–	–	–
22	266.4	266.3	–	285	219.2	218.1	–	213	–
23	279.9	280.4	–	296	222.9	222.2	–	–	–
24	308.5	308.5	–	319	246.5	245.1	–	243	239
25	323.9	323.3	–	326	259.1	258.6	–	267	**270**
26	335.0	335.1	–	345	285.6	285.8	–	298	–
27	356.8	355.7	–	368	295.3	297.5	–	323	–
28	377.9	376.4	–	377	323.6	322.5	–	–	327
29	399.2	400.5	–	400	337.3	335.3	–	–	353
30	418.6	420.3	–	–	365.2	363.5	–	386	388
31	424.0	424.8	–	–	402.3	402.6	–	–	–
32	428.6	432.0	–	427	411.3	413.0	–	–	–
33	436.3	442.5	–	432	417.9	418.0	–	415	**416**
34	440.8	446.8	–	442	419.2	420.5	–	424	**425**
35	442.9	448.0	–	452	438.3	438.8	–	443	–
36	445.4	451.1	–	458	453.1	458.0	–	–	451
37	452.3	458.8	–	474	456.6	465.0	–	–	–
38	454.7	461.0	–	480	464.9	472.2	–	–	–
39	476.6	477.9	–	487	471.6	477.2	–	480	**479**
40	480.0	484.5	–	491	473.3	478.4	δC–N	–	–
41	489.8	494.3	–	497	483.8	486.5	δC–N	–	–
42	502.6	506.6	–	514/522	487.9	492.1	–	–	501
43	541.4	540.2	–	551	527.6	526.6	–	537	536
44	583.4	585.4	–	600	576.1	575.9	–	–	588

Table 3. (*Continued*)

	Low-spin state				High-spin state				
	Calculated wavenumber (cm^{-1})			Experimental (cm^{-1})	Calculated wavenumber (cm^{-1})			Experimental (cm^{-1})	
Mode no.	TZVP	TZVPP	Assignment	Raman	TZVP	TZVPP	Assignment	Raman	FT-IR
45	616.9	615.7	–	–	613.1	611.0	νC–C (6a)	–	–
46	637.7	634.6	–	622	620.5	618.4	νC–C (6a)	618	–
47	640.6	637.3	–	**645**	629.8	627.2	νC–C (6a)	637	–
48	643.6	642.2	–	**651**	635.7	633.7	νC–C (6a)	644	**642**
49	651.4	649.1	–	**658**	645.3	643.6	νC–C (6a)	650	–
50	700.3	711.5	–	720	708.6	722.8	–	722	721
51	715.1	727.4	–	740	717.6	733.6	–	–	738
52	731.5	744.1	–	759/751	728.2	741.3	ωCH (11)	–	748
53	737.8	746.6	–	763	740.8	744.2	ωCH (11)	–	–
54	743.3	749.4	–	770	743.8	747.3	ωCH (11)	–	**759**
55	744.6	752.9	–	782	747.5	752.1	ωCH (11)	763	–
56	770.5	770.7	–	792	770.3	771.3	–	781	780
57	802.5	803.4	–	803	803.9	806.3	–	797	796
58	823.4	823.9	–	819	819.7	824.9	–	814	812
59	830.1	833.0	–	830	824.1	828.0	Fe–(NC)–S	837/831	–
60	833.5	838.6	Fe–(NC)–S	–	834.6	834.9	τCH (10b)	848	848
61	835.5	843.0	Fe–(NC)–S	**838**	867.1	871.8	τCH (10b)	861	–
62	856.3	864.7	τCH (10b)	**850**	868.2	874.9	τCH (10b)	871	–
63	863.7	870.0	τCH (10b)	865	869.4	877.7	Fe–(NC)–S	884	–
64	864.6	871.1	τCH (10b)	877	874.0	882.2	τCH (10b)	892	889
				C–H out of plane					
65	904.4	906.3	–	887	910.6	911.6	–	–	–
66	918.7	921.8	–	890	930.7	932.7	–	930	927
67	928.1	939.0	τCH (17)	929	937.3	945.2	–	940	939
68	932.0	941.7	τCH (17)	–	940.3	949.3	–	945	–
69	938.9	948.9	τCH (17)	938	942.9	952.2	τCH (17)	951	–
70	950.6	955.1	τCH (5)	–	956.1	962.4	–	962	960
71	953.4	973.0	τCH (5)	953	958.5	976.3	τCH (5)	–	971
72	960.5	974.6	τCH (5)	961	962.8	976.6	τCH (5)	975	977
73	963.6	977.9	τCH (5)	976	966.3	979.2	τCH (5)	–	–
74	978.8	980.5	τCH (5)	987	978.3	985.2	τCH (5)	–	–
75	1001.2	1001.0	ρCH (12)	999	988.9	989.3	ρCH (12)	996	995
76	1006.3	1006.1	ρCH (12)	1002	998.2	998.1	ρCH (12)	1016	**1018**
77	1011.3	1012.1	ρCH (12)	1016	999.6	999.6	ρCH (12)	**1019**	–
78	1016.5	1016.9	νC–C, C–N	**1024**	1021.6	1023.4	νC–C, C–N	–	–
79	1044.3	1044.7	ρCH (18a)	**1032**	1044.1	1044.2	ρCH (18a)	1031	–
80	1046.2	1046.7	ρCH (18a)	1050	1046.4	1045.8	ρCH (18a)	1050	1048
81	1059.8	1060.6	ρCH (18a)	1061	1053.1	1053.4	ρCH (18a)	1064/1057	1056
82	1070.6	1070.3	νC–C, C–N	1071	1083.2	1083.2	νC–C, C–N	1085	**1084**
83	1090.9	1091.1	νC–C, C–N	1083	1093.4	1093.1	ρCH (18b)	–	–
84	1098.3	1097.5	ρCH (18b)	1104	1098.5	1097.1	ρCH (18b)	1105	1104
85	1102.3	1101.2	ρCH (18b)	1$\overline{1}$10	1100.9	1099.5	ρCH (18b)	1116	1115
86	1105.0	1104.1	ρCH (18b)		1106.7	1105.5	νC–N τC–H$_2$		
87	1148.1	1144.5	ρCH (15)	1151	1147.9	1144.7	ρCH (15)	1151	**1150**
88	1151.5	1147.4	ρCH (15)	1$\overline{1}$58	1153.4	1148.1	ρCH (15)	1156	**1155**
89	1153.5	1149.7	ρCH (15)		1154.1	1149.1	ρCH (15)		

(*continued overleaf*)

Table 3. (*Continued*)

	Low-spin state				High-spin state				
	Calculated wavenumber (cm^{-1})			Experimental (cm^{-1})	Calculated wavenumber (cm^{-1})			Experimental (cm^{-1})	
Mode no.	TZVP	TZVPP	Assignment	Raman	TZVP	TZVPP	Assignment	Raman	FT-IR
90	1192.4	1190.5	–	–	1192.9	1190.9	–	–	–
91	1198.1	1196.6	–	1214	1200.4	1200.6	–	1203	1202
92	1206.2	1206.0	τC–H$_2$	1224	1205.4	1204.7	τC–H$_2$	1215	1224
93	1219.6	1218.8	–	1228	1219.3	1218.2	–	1219	1239
94	1228.3	1227.2	νC–C	1236	1235.8	1234.3	νC–C	1226	1253
95	1243.5	1243.4	–	1249	1250.7	1249.1	–	1253	–
96	1249.7	1246.3	–	–	1256.7	1252.9	–	–	–
97	1266.7	1267.7	ρCH (9b)	1254	1273.6	1275.5	ρCH (9b)	1272	1272
98	1267.2	1267.8	ρCH (9b)	1270	1275.2	1278.3	ρCH (9b)	1280	1278
99	1271.8	1274.0	ρCH (9b)	1276	1278.5	1279.4	ρCH (9b)		
100	1284.6	1286.5	ρCH (14)	1286	1288.5	1290.5	ρCH (14)	1295	1294
101	1293.5	1292.8	ρCH (14)	1303	1300.5	1300.5	ρCH (14)	1310	**1308**
102	1302.9	1301.9	ρCH (14)	1313	1309.3	1308.4	ρCH (14)	1317	1316
103	1340.2	1337.2	ρCH (3)	1358	1347.2	1344.1	ρCH (3)	1366	1356
104	1345.3	1343.2	ρCH (3)	1364	1349.9	1346.2	ρCH (3)	1379	1377
105	1358.2	1355.5	ρCH (3)	1377	1362.4	1359.5	ρCH (3)		
106	1369.9	1366.6	ωC–H$_2$	1381	1369.9	1367.4	ωC–H$_2$	–	–
107	1409.9	1406.7	δC–H$_2$	1417	1414.1	1410.8	δC–H$_2$	–	–
108	1423.5	1421.5	δC–H$_2$	–	1425.9	1425.5	νCC (19b)		
109	1429.3	1428.1	νCC (19b)	1435	1427.4	1426.2	νCC (19b)	1423	1425
110	1430.5	1429.2	νCC (19b)	–	1428.2	1428.1	νCC (19b)	–	–
111	1431.3	1431.3	νCC (19b)	–	1435.2	1431.3	δC–H$_2$	**1438**	**1435**
112	1440.8	1438.0	δC–H$_2$	1447	1437.5	1433.9	δC–H$_2$	1446	1441
113	1445.4	1443.4	δC–H$_2$	1455	1445.9	1444.4	δC–H$_2$		
114	1454.4	1455.9	νCC (19a)	1468	1455.8	1457.5	νCC (19a)	1455	1458
115	1457.4	1458.9	νCC (19a)	1480	1461.8	1462.4	νCC (19a)	1472	1473
116	1462.1	1463.4	νCC (19a)	1486	1464.9	1466.6	νCC (19a)	1484	1484
117	1535.1	1537.9	νCC (8b)	1569	1545.2	1549.5	νCC (8b)	1572	1571
118	1553.4	1555.3	νCC (8b)	–	1554.2	1556.5	νCC (8b)	–	–
119	1555.5	1557.3	νCC (8b)	–	1555.8	1558.8	νCC (8b)		
120	1586.1	1587.8	νCC (8a)	1600	1578.1	1580.4	νCC (8a)	1591	1594
121	1590.0	1591.7	νCC (8a)	**1606**	1582.9	1585.4	νCC (8a)	1604	1603
122	1595.1	1596.6	νCC (8a)	**1609**	1587.4	1589.3	νCC (8a)		
123	2085.2	2080.3	νC–N as	**2104**	2029.8	2023.7	νC–N as	**2065**	**2065**
124	2101.3	2093.1	νC–N sy	**2117**	2046.3	2041.0	νC–N sy	**2076**	**2076**
				νC–H aliphatic					
125	2931.2	2930.5	νC–H	2864	2909.1	2897.3	νC–H	2854	2850
126	2934.8	2933.7	νC–H	2898	2900.9	2898.4	νC–H	2859	2858
127	2963.9	2962.9	νC–H	2915	2921.3	2917.6	νC–H	2896	2890
128	2988.3	2985.2	νC–H	2930	2982.8	2981.0	νC–H	–	2908
129	3004.3	3000.9	νC–H	**2936**	2990.3	2987.4	νC–H	**2933**	2928
130	3010.1	3007.3	νC–H	**2940**	3001.6	3000.5	νC–H	–	2947
131	3022.8	3019.2	νC–H	**2952**	3004.9	3006.5	νC–H	2961	–
132	3031.2	3028.2	νC–H	2973	3025.7	3025.2	νC–H	–	–

Table 3. (*Continued*)

Mode no.	Low-spin state					High-spin state				
	Calculated wavenumber (cm^{-1})			Experimental (cm^{-1})		Calculated wavenumber (cm^{-1})			Experimental (cm^{-1})	
	TZVP	TZVPP	Assignment	Raman		TZVP	TZVPP	Assignment	Raman	FT-IR
				νC−H aromatic P1 P2 P3						
133	3109.8	3109.9	νC−H (13)			3104.4	3102.7	νC−H (13)		3024
134	3110.7	3110.0	νC−H (13)	3035		3106.9	3105.4	νC−H (13)	3033	
135	3113.4	3113.3	νC−H (13)	3049		3109.9	3108.9	νC−H (13)	3057	
136	3122.6	3123.0	νC−H (7a)	**3065**		3112.8	3110.6	νC−H (7a)	**3065**	3064
137	3123.8	3123.3	νC−H (7a)			3115.1	3113.0	νC−H (7a)		
138	3125.6	3125.8	νC−H (7a)	3074		3118.4	3116.8	νC−H (7a)	3077	
139	3134.1	3134.1	νC−H (20a)			3121.7	3120.6	νC−H (20a)	3096	
140	3135.1	3134.7	νC−H (20a)	3082		3122.4	3121.1	νC−H (20a)		
141	3136.3	3136.2	νC−H (20a)	3089		3124.6	3123.9	νC−H (20a)	3140	
142	3145.7	3144.4	νC−H (2)	3102		3133.9	3133.1	νC−H (2)		
143	3150.4	3148.7	νC−H (2)	3135		3136.2	3136.0	νC−H (2)		
144	3163.5	3161.2	νC−H (2)			3137.0	3137.1	νC−H (2)		

Figure 4. IR and Raman spectra of the pmea ligand and Raman spectrum of [Fe(pmea)(NCS)$_2$] (both Raman spectra recorded with λ_{ex} = 785 nm).

to HS transition. And this is indeed the case. The two C═C stretching modes give rise to two well-separated, moderately intense bands at 1571/1603 cm^{-1} (HS) and 1572/1604 cm^{-1}, respectively. A band contour analysis yields here (and also for other 'broad' bands) further contributions of low intensity, which are also included in Table 3.

In the spectral range between 1000 and 1100 cm^{-1}, the spectra of the complex displayed in Fig. 3 only show one stronger band instead of the two observed in the spectra of the ligand. But the SERS spectra of pyridine adsorbed on Ag, Au or Cu show a similar band pattern around 1000 cm^{-1} as the complex.[35,36] Wu *et al.*[35] stated that 'the spectral features of pyridine on metal surfaces are really complicated. So far, no satisfactory assignments of the vibrational modes have been achieved'. Their accompanying calculations suggest that the coupling among ν_1, ν_{12} and

ν_{18a} modes and the coupling between these modes and the N-metal bond depend on the strength of the N-metal bond. One major problem in achieving a quantitative explanation of the SERS spectra is the lack of knowledge of the adsorption geometry and the mode of binding. Because the structure of the complexes investigated here is well defined, the analysis of the calculated normal coordinates should also be very valuable for the discussion and band assignment of pyridine interacting with a metal (ion).

The maximum of the most intense peak shifts from about 1032 cm^{-1} (LS) to 1019 cm^{-1} (HS), but the band contour analysis again yields several bands of low intensity with similar wavenumbers in both spectra (Fig. 5). A simple-minded model could explain such a hypsochromic shift of the pyridine-breathing mode by the restrictions posed upon the movement of the pyridine nitrogen because of the binding to the central metal ion, which is stronger in the LS than in the HS state (compare also bond lengths in Table 1).

Whereas the assignment of the vibrations discussed above is fairly unique, the identification of the other corresponding pairs of vibrational bands in the HS and LS state, respectively, is difficult and can therefore be performed only by comparison with the results of the quantum-chemical calculations (see below). It is remarkable that the Raman spectrum of the LS complex exhibits five bands in the range 50–100 cm^{-1} whereas the HS complex shows only one band. This trend continues for wavenumbers up to about 500 cm^{-1}. Since the location of some of the bands observed for the LS complex matches the location of bands observed for the HS complex, one can question whether these are actually due to remainders of molecules in the HS state. But judged by the intensity ratio of the well-separated C═NS bands one can exclude this possibility.

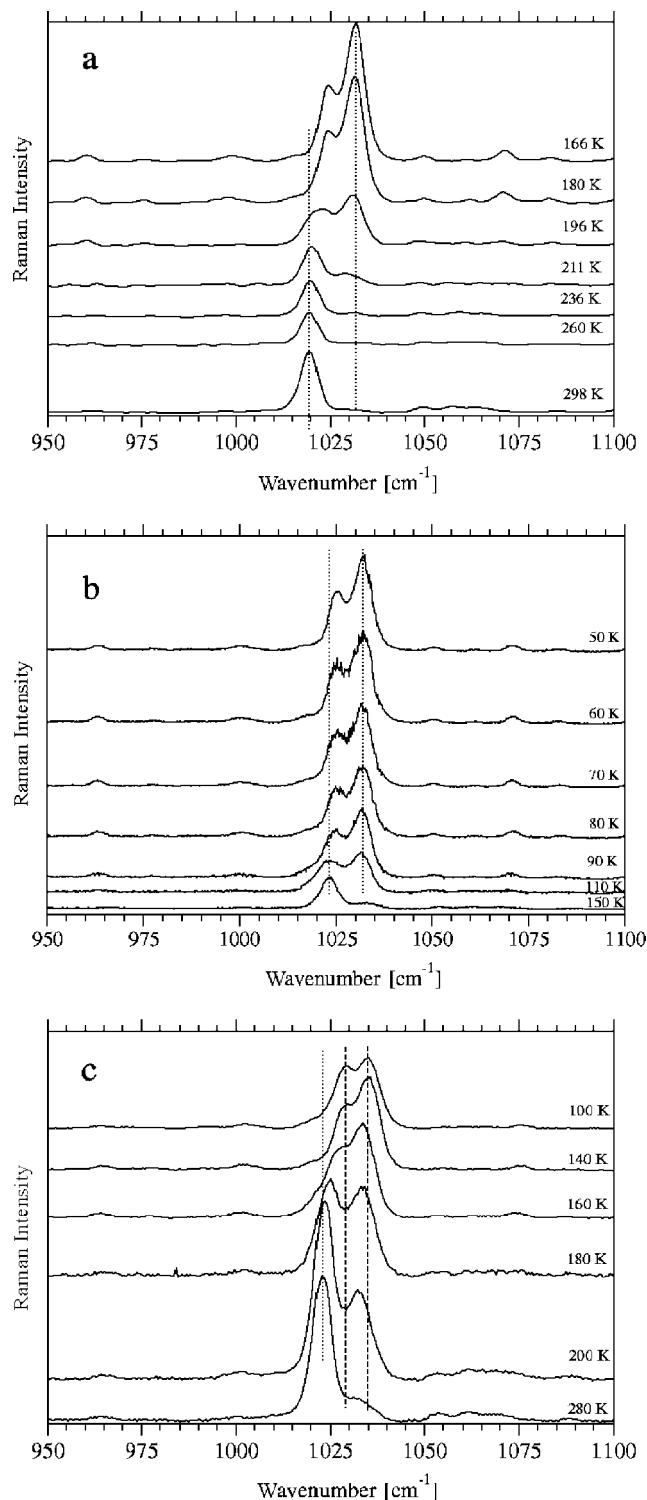**Figure 5.** Section of the Raman spectra of [Fe(pmea)(NCS)$_2$] showing pyridine breathing and deformation modes recorded at different temperatures: (a) $\lambda_{ex} = 1064$ nm; (b) $\lambda_{ex} = 785$ nm and (c) $\lambda_{ex} = 514.5$ nm.

The Raman spectra recorded at different temperatures reveal additional insight into the structural changes

accompanying the LS to HS transition. As mentioned above, the symmetric and antisymmetric C=NS vibrations of the LS complex show at about 2117 and 2104 cm^{-1}, respectively. These band positions are conserved until the conversion temperature T_c is approached (Fig. 6(a)). For temperatures above T_c, the bands originating from the LS complex become rather weak, but nevertheless one can conclude beyond doubt that the band positions are shifted by about 7 cm^{-1} towards lower wavenumbers. A similar trend is found for the bands characterising the HS complex. Again, the band positions (2082 and 2069 cm^{-1}) seem to be conserved for temperatures below T_c, but shift by about 5 cm^{-1} towards smaller wavenumbers in the temperature regime just above T_c. At higher temperatures (i.e. when the LS complex does not contribute to the spectra anymore), the band positions adopt the final values that are reported in Table 3 (2076 and 1065 cm^{-1}). Our tentative explanation for these shifts is that upon the LS to HS transition not only the inner coordinates
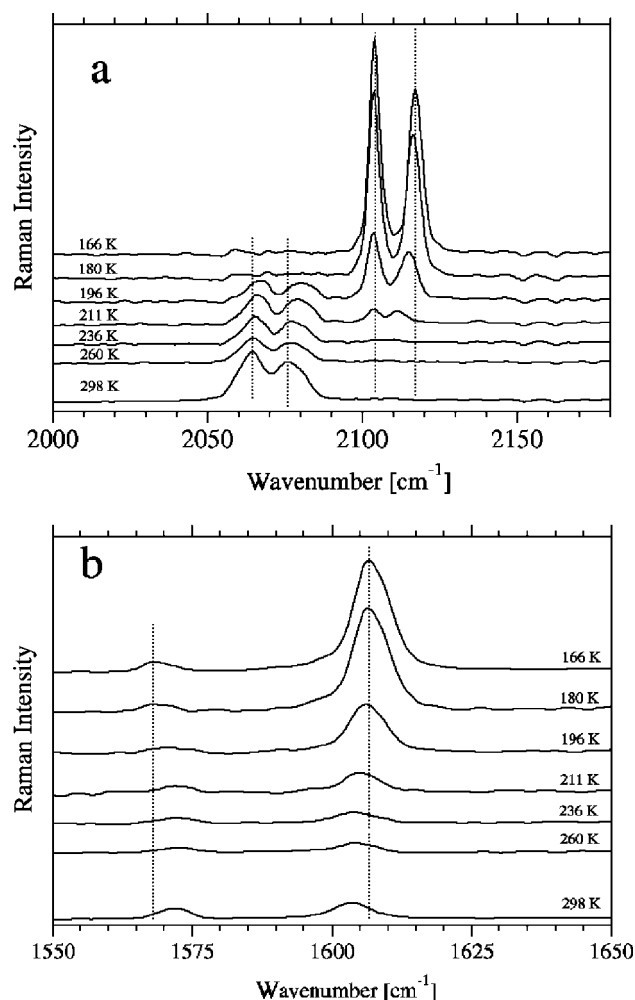

Figure 6. Section of the NIR-FT Raman spectra of [Fe(pmea)(NCS)$_2$] recorded at different temperatures: (a) C=NS stretching vibrations; (b) C=C stretching vibrations of pyridines.

of the individual molecules change, but also the distances of the CNS groups to their nearest neighbour molecules. In this context, it is also worth noticing that the width of the CNS bands is larger for the HS complex thus indicating an inhomogeneous broadening.

Although the shifts between the (thermalized) LS and HS complexes are smaller in case of the pyridine C=C-stretching modes, the effect described above for the C=NS-stretching modes can also be verified (Fig. 6(b)).

Similar shifts of the position of the C=NS Raman bands with temperature are observed when either the 785-nm radiation of a Ti:Sapphire laser (300 mW) or the 514.5-nm radiation of an Ar^+ laser (50 mW) is used for excitation. To avoid (photo-) thermal degradation of the sample, the $[Fe(pmea)(NCS)_2]$ complex is diluted in a KBr matrix as described above. This implies that the temperature gradient across the sample (probed volume) can be different from one sample to the next. Furthermore, the size of the micro-crystals can be different because the samples investigated stem from different charges.

The spectra recorded with 785-nm radiation excitation (Fig. 7(a)) differ in several aspects from those shown in Fig. 6(a) (1064 nm). The location of the antisymmetric C=NS vibration of the LS complex ($2104\,cm^{-1}$) is independent of the sample temperature, whereas the symmetric C=NS vibration shifts from about $2020\,cm^{-1}$ (13 K) to $2016\,cm^{-1}$ ($T \geq 110$ K). Around 60 K, a band pair appears that can be assigned to the antisymmetric ($2072\,cm^{-1}$) and symmetric ($2088\,cm^{-1}$) C=NS vibration. The former band shows a small shift towards lower wavenumbers when the temperature setting is raised to about 100 K. The latter band is very wide and is most likely a superposition of two closely spaced bands. The position of the two constituent bands seems to be conserved, but their relative intensities change with temperature thus giving the impression of a band shift. We take this observation as additional evidence that with the LS to HS transition not only the intra-molecular but also the inter-molecular distances (and concomitantly the size of the interactions) change.

The hypothesis of changes of intra-molecular and inter-molecular distances is supported also by the spectra recorded from a third sample with 514.5 nm excitation (Fig. 7(b)). The positions of all four characteristic C=NS bands are conserved when the temperature setting is kept below 140 K. But a sudden jump of the positions of the symmetric C=NS vibrations of both the LS- and HS-complex towards smaller wavenumbers occurs when the conversion temperature is approached.

DISCUSSION

Effect of inter-molecular interactions on the wavenumber of the C=NS stretching vibrations

A crucial test for the validity of the calculations and justification for considering an isolated molecule only is
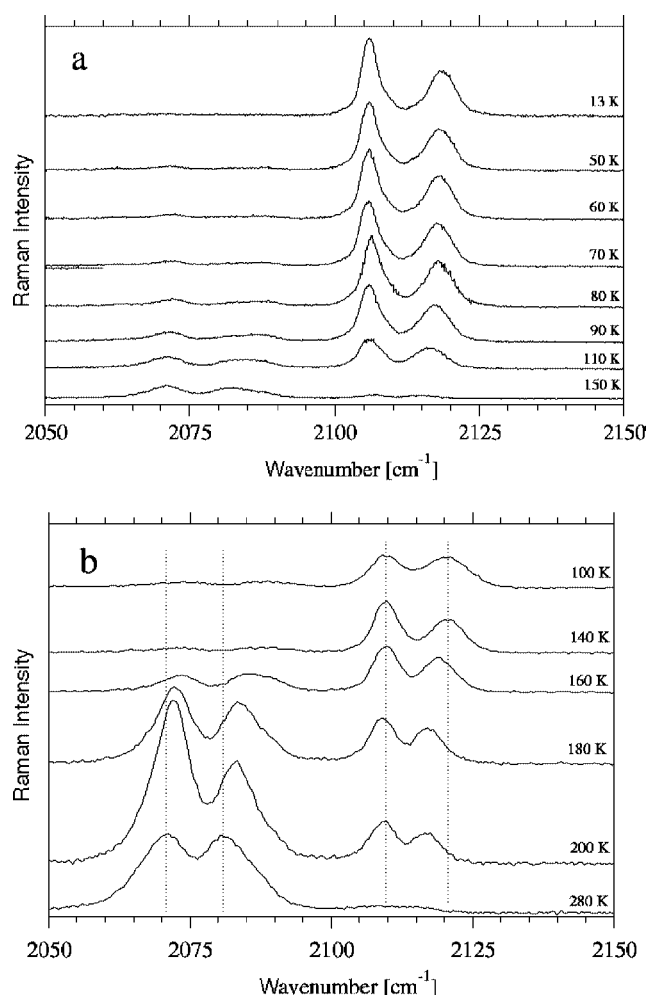

Figure 7. Section of the Raman spectra of $[Fe(pmea)(NCS)_2]$ showing N=CS stretching modes recorded at different temperatures: (a) λ_{ex} = 785 nm; (b) λ_{ex} = 514.5 nm.

the correct prediction of the position and shift of the uniquely identified $(N=CS)_2$ stretching vibrations. For the LS complex, the symmetric and antisymmetric stretching vibrations are predicted (TZVP/TZVPP) at $2101/2093\,cm^{-1}$ and $2085/2080\,cm^{-1}$, respectively. In the Raman spectrum, two strong bands are observed around $2117\,cm^{-1}$ and $2104\,cm^{-1}$. For the HS complex, the corresponding pair of bands is predicted at 2046/2041 and $2030/2024\,cm^{-1}$ whereas the experimental values are 2076 and $2065\,cm^{-1}$. In conclusion, experimental and calculated wavenumbers differ for these modes for the LS complex by about 16/24 (s) and 19/24 (as) cm^{-1} and for the HS complex by about 30/35 (s) and 35/41 (as) cm^{-1}, respectively. Since the accuracy of wavenumbers obtained from harmonic BP86/RI/TZVP(P) force fields can, however, be better than $10\,cm^{-1}$ for large Fe(II) and Ru(II) complexes[37,38] because of the above mentioned error compensation, we may conclude that at least part of the differences originates from the neglect of the actual intermolecular interactions in the crystal.

In our previous investigation of [Fe(phen)$_2$(NCS)$_2$], experimental and calculated wavenumbers differed by more than 50 cm^{-1}. When we included in a model calculation the interaction of the CNS groups with the nearest neighbour molecule the calculated wavenumbers increased by about 40 cm^{-1} in the right direction. In the [Fe(pmea)(NCS)$_2$] crystal, the distances of the sulphur atoms to the closest carbon atoms of the various pyridine moieties are of the same magnitude as in case of [Fe(phen)$_2$(NCS)$_2$]: D [S(axial) − C] ∼ 350 pm, D [S(equatorial) − C] ∼ 390 pm.

We therefore suggest that in [Fe(pmea)(NCS)$_2$] there is also a considerable interaction between the CNS groups and their nearest neighbour molecule. This interaction is obviously larger in the HS complex (larger differences between experimental and calculated wavenumbers) because of a rearrangement of the interacting groups. The band shifts observed, when the conversion temperature is approached, could indicate a rearrangement of the components of one unit cell if the molecules in the neighbouring unit cell change their spin state.

Assignment of vibrational bands

In previous work,[3,34,37,38] iron-ligand bond stretching vibrations could be identified by means of isotope substitution. Accordingly, they should be found in the range 400–500 cm^{-1} for the LS isomer and in the wavenumber range 250–300 cm^{-1} for the HS isomer. Inspection of the normal coordinate pictures reveals, however, that in our compound, several modes that exhibit a large movement of the iron atom relative to the attached ensemble of ligands are found below the spectral region mentioned above (e.g. modes no. 12, 13, 15). The generally adopted assumption of a decrease in the stretching wavenumber of the metal-to-ligand bonds upon LS to HS transition is verified for these modes. But for other modes, it is rather difficult, if not impossible, to make a generally valid statement about the wavenumber shifts correlated with the LS to HS transition of the central metal. A closer inspection of the normal mode coordinates shows that the mixing pattern of local movements in the ligands is different in the LS and HS isomer. This can be rationalized in a simple picture. If the bond strength is increased and concomitantly the wavenumbers of the localized metal-to-ligand stretching vibration then this mode will preferentially couple with those local modes of the ligands, whose wavenumber is also higher. As a further consequence, the mixing pattern of all other small wavenumber modes will also change. Therefore, one finds nearly no band below about 400 cm^{-1} whose predicted wavenumber is not changed by more than about 30 cm^{-1} if one just compares the vibrations with the same mode number. The analysis of the normal coordinates shows, however, that some modes that are essentially conserved upon the LS to HS transition appear with a different mode number because of the shift of the spin-state sensitive modes (e.g. modes no. 60/61 LS and 59/63 HS).

In our example, we find two bands in the above cited wavenumber range (LS: 400–500 cm^{-1}, HS: 250–300 cm^{-1}) that are connected with a movement of the iron relative to the ensemble of ligands (LS: modes no. 28 and 30, HS: modes no. 25 and 27). The other normal coordinates involve large deflections in the ligands, especially in the two CNS groups. Noteworthy is, that in the HS complex the angle deformation modes (no. 37, 38, 40, 41) are localized on either one of the two CNS ligands, whereas in the LS complex linear combinations of motions of both ligands appear (no. 33, 35, 36, 38). This different mixing pattern for LS and HS complex, which is also found for other 'corresponding' modes, could influence the scattering cross section and be the cause that more bands are found in the Raman spectra of the LS complex than in those of the HS complex.

In the spectral regions above about 600 cm^{-1} one can find several groups of vibrations, which are well separated from each other. In part they are correlated with certain types of normal coordinates of the pyridine moieties as indicated in Table 3. The first such group to be discussed consists of modes 43–49. Modes 46–49 represent different linear combinations of the 652 cm^{-1} pyridine mode. 46: P2, 47: P1 − P3, 48: P1 + P3 (+, − indicate in-phase and out-of-phase linear combinations, respectively).

Most of the bands observed between 700 and 750 and 900 and 980 cm^{-1}, respectively, can be assigned – by comparison with the calculated normal coordinates – to hydrogen out-of-plane motions (in-phase and out-of-phase) of the pyridine moieties. In contrast with other spectral regions, each of these normal modes is located on one pyridine only, obviously because the coupling between the three pyridines is small for this type of vibrations.

But as already mentioned above, a strong mixing is suggested between the ring breathing (ν_1), the ring deformation (ν_{12}), and the C–H in-plane bending modes (ν_{18}) of the three pyridines (Fig. 8). The mixing pattern supposedly changes with the strength of the interaction of the ligating N-atoms and the central metal induced by the LS to HS transition. Consequently, one must be cautious when making up a correlation between bands observed in the spectra of the LS and HS complex. The normal coordinate pictures of modes 71–78 suggest that the modes 71–74 represent essentially motions of hydrogen atoms only and can therefore not be associated with the ring-breathing mode of pyridine. Of the modes 75–78, on the other hand, three must be characterized as linear combination of the pyridine ring deformation mode ν_{12}, and the fourth as N(amino)-(CH$_2$) stretch. Modes 79–81 represent, as may be expected, linear combinations of C–H i.p. bending modes of pyridine. Like in other cases, in which one type of pyridine normal coordinates forms linear combinations in the complex, it is difficult to assign an experimentally observed band to a specific linear combination. Therefore, in Table 3 we did not make a correlation between specific modes but rather
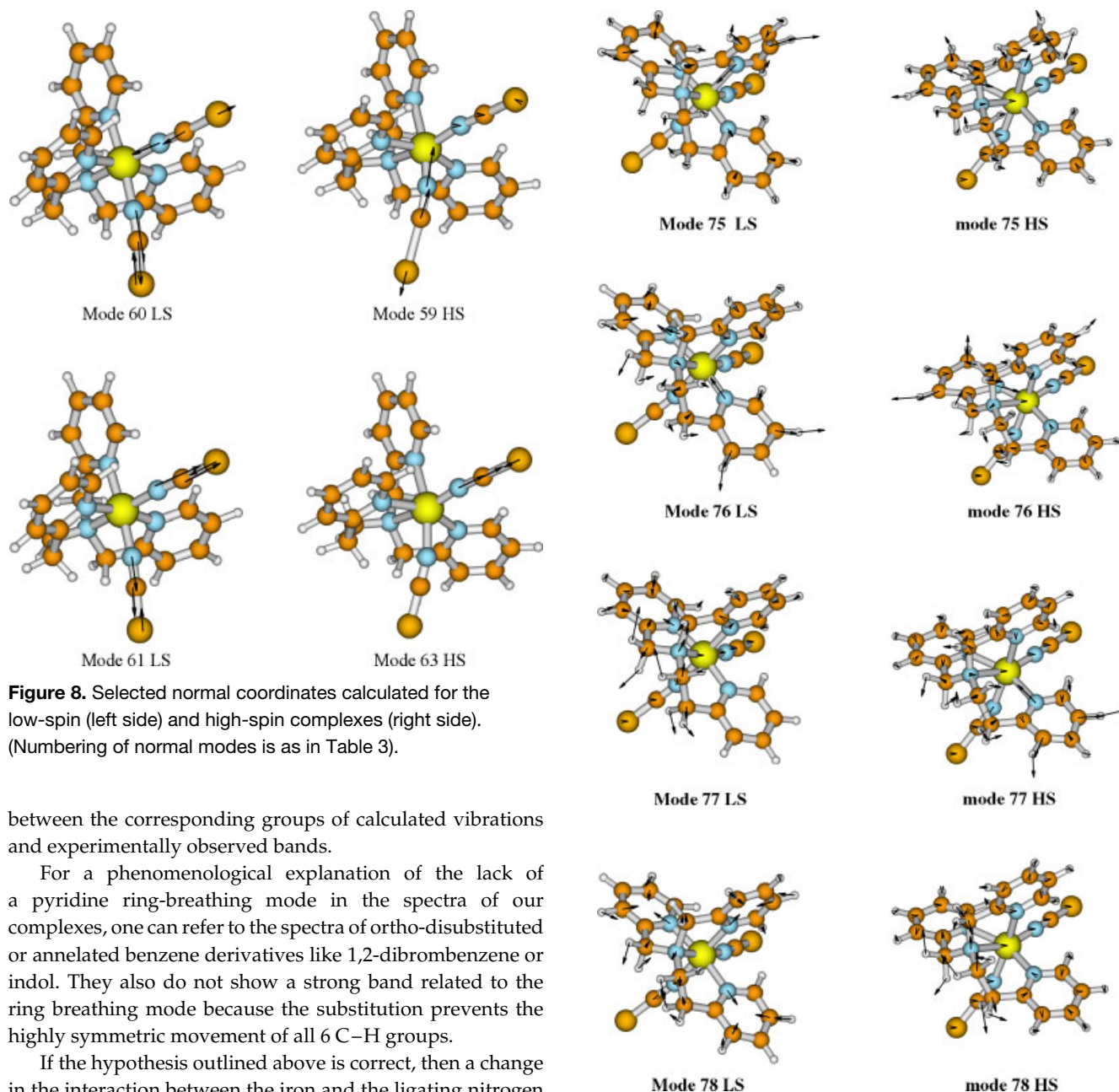
Mode 60 LS   Mode 59 HS

Mode 61 LS   Mode 63 HS

Figure 8. Selected normal coordinates calculated for the low-spin (left side) and high-spin complexes (right side). (Numbering of normal modes is as in Table 3).

Mode 75 LS   mode 75 HS

Mode 76 LS   mode 76 HS

Mode 77 LS   mode 77 HS

Mode 78 LS   mode 78 HS

Figure 8. (*Continued*).

between the corresponding groups of calculated vibrations and experimentally observed bands.

For a phenomenological explanation of the lack of a pyridine ring-breathing mode in the spectra of our complexes, one can refer to the spectra of ortho-disubstituted or annelated benzene derivatives like 1,2-dibrombenzene or indol. They also do not show a strong band related to the ring breathing mode because the substitution prevents the highly symmetric movement of all 6 C–H groups.

If the hypothesis outlined above is correct, then a change in the interaction between the iron and the ligating nitrogen atoms can also be induced in a certain molecule, if molecules in the neighbourhood undergo a LS to HS transition and thus explain the broadening or shifting of bands once the transition temperature is approached.

Those normal modes that represent either essentially (out-of-phase) hydrogen in-plane motions of the pyridine ligands or motions of the hydrogens of the (CH$_2$) groups are found in the spectral range 1150 to 1450 cm^{-1}. Their wavenumbers barely change upon the LS to HS transition.

The aromatic C–C(N) stretching vibrations cause three band triplets associated with modes 114–122. Here again the normal coordinate pictures allow a description as linear combination of modes localized on the three pyridines, although with a different mixing pattern: e.g. mode no. 120:

P2 − (P1 + P3), 121: P1 − P3, 122: P3 + P2 + P1. Without a reliable calculation of the IR and Raman intensities an assignment of the experimental bands to a specific normal coordinate is impossible. Since the (totally) symmetric vibrations generally exhibit the largest Raman intensities it is tempting to correlate the more intense Raman bands to those linear combinations, which have the 'most symmetric pattern' of deviations from equilibrium geometry. With such an assignment accepted, the calculations predict a downward shift of 7.3 cm^{-1} for mode 122 and an upward shift of 1.3 cm^{-1} for mode 119, in good agreement with the experimentally
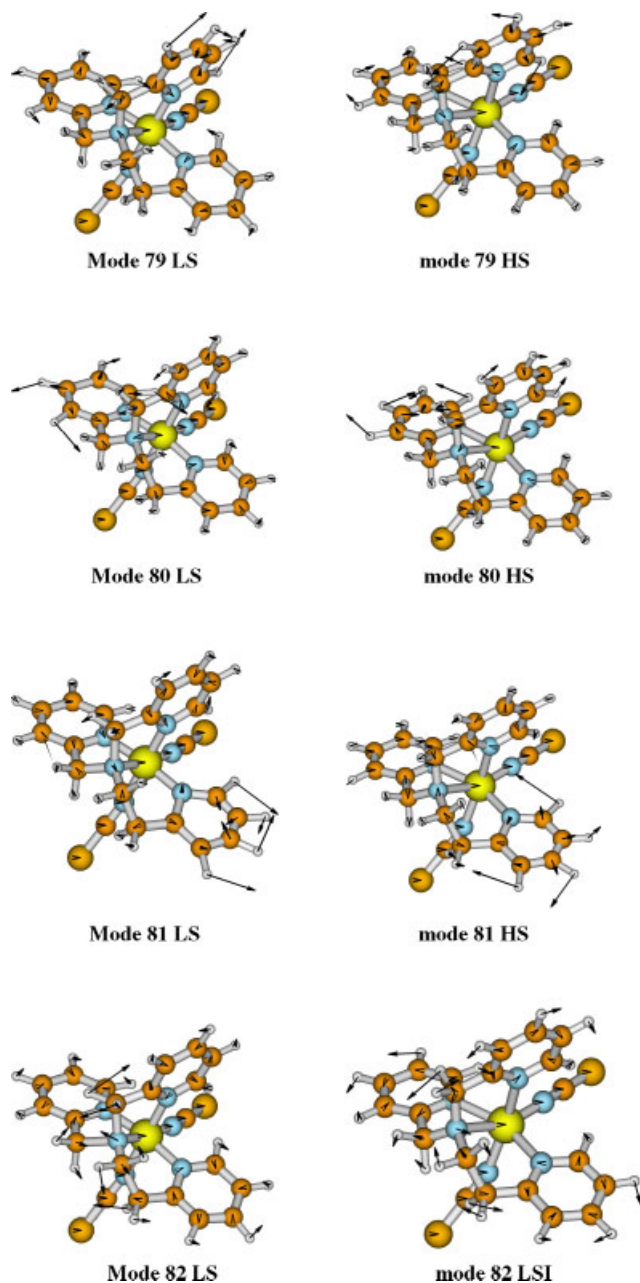
Figure 8. (*Continued*).

observed shifts of −5 and +4 cm^{-1}, respectively. This and the fair matching of the absolute wavenumbers provide evidence for the (general) high quality of the calculated wavenumbers. This judgement is confirmed also by the reproduction of the wavenumbers of those modes, which can be correlated with high fidelity.

According to the calculations, the aliphatic and aromatic C−H stretching vibrations are well separated, which facilitates the assignment of the experimental bands considerably. The wavenumbers of these modes are often calculated at values that are too high, especially for Hartree-Fock force fields calculated with small basis sets. Therefore,

a factor of 0.89 is usually applied in such calculations for a better comparison with experimental numbers.[39] We decided, however, to present the unscaled wavenumbers to avoid a discussion of the correction factor.

A final remark must be devoted to the vibrations with wavenumbers below 100 cm^{-1}. Since the intensities of these bands are already low in the spectrum of the LS complex, we cannot exclude the possibility that the 'corresponding' bands of the HS complex are even weaker and therefore not accessible for experimental reasons. Such changes of intensity have been discussed above as a possible consequence of a different mixing pattern of internal coordinates. Inspection of the calculated normal coordinates reveals that these extremely low wavenumber modes are in part due to a movement of the constituent moieties relative to each other, for example, in one case, a whole pyridine seems to rotate around the Fe−N bond. Such a movement should be highly anharmonic because of the clamping action of the (CH$_2$) group(s). Consequently, one must not be surprised if overtones show up in the spectra of the LS complex with stronger Fe−N bonds.

Calculation of the entropy change ΔS_{vib} associated with the LS to HS transition

The vibrational contribution to the entropy can be calculated from the frequencies $\nu_i = c \times \tilde{\nu}_i$ in the harmonic approximation according to:

$$S_{vib} = \sum_i \{h\nu_i/kT[\exp(h\nu_i/kT) - 1]^{-1}$$
$$- \ln[1 - \exp(-h\nu_i/kT)]\} \qquad (1)$$

With the two sets of calculated wavenumbers we can evaluate different estimates. From the complete set of calculated normal mode wavenumbers produced with the TZVP basis set for the LS and HS state, we obtain a vibration-related entropy change of 26.8 J/(mol·K), while the larger TZVPP basis sets yields $\Delta S_{vib} = 40.3$ J/(mol·K).

To illustrate the magnitude of the contribution of the various normal modes to ΔS_{vib} we have displayed in Fig. 9 the total vibronic entropy of the LS and HS state, respectively, as a function of the number of normal modes included in the calculation. As reported earlier for the complex [Fe(phen)$_2$(NCS)$_2$], consideration of only the very low wavenumber modes yields a negative value for the entropy change. However, if modes above 100 cm^{-1} are also included in the estimation, then a positive value results. Figure 9 also clearly demonstrates that the modes with wavenumbers between 100 and 450 cm^{-1} contribute significantly to ΔS_{vib}. This is in accordance with the simplified picture that the modes in this spectral region are modified strongly by the change in the strength of the metal−N(ligand) bond.

In our previous publication we reported $\Delta S_{vib} \sim 19.5$ J/(mol·K) for the complex [Fe(phen)$_2$(NCS)$_2$] based on calculations employing the TZVP basis set. Since this value was
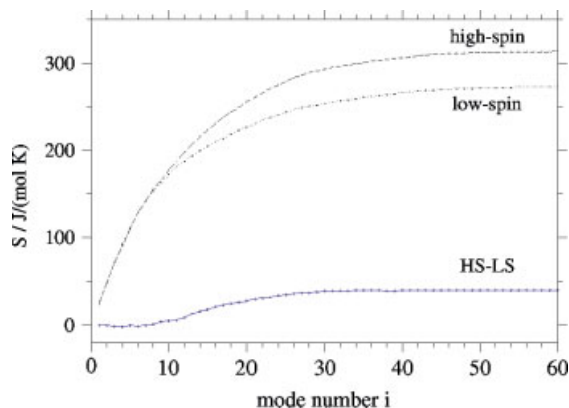
Figure 9. Vibrational entropy of the low-spin (LS, · · · ·) and high-spin (HS, - - - -) complexes, with the normal modes included in the estimation up to the ith mode. Additionally, the entropy change $S_i(HS) - S_i(LS)$ is shown (— · —).

too small to explain the experimentally determined value of $\Delta S_{tot} \sim 50$ J/(mol·K), we concluded, in accordance with Paulsen *et al.*,[37,38] that optical phonons must give rise to a significant entropy increase upon the LS to HS transition. The results presented now for [Fe(pmea)(NCS)$_2$] suggest that the larger TZVPP basis set should be used instead of the TZVP basis for a calculation of the low wavenumber modes that contribute an essential fraction to ΔS_{vib}.

SUMMARY AND CONCLUSION

DFT calculations employing the BP86 functional and two different basis sets were performed to calculate the geometries and normal modes of the novel spin crossover complex [Fe(pmea)(NCS)$_2$] in both the LS and HS state. The differences between the structural parameters of the calculated isolated complex and the X-ray data suggest that crystal-packing forces influence the geometry in the solid state. They are assumed to provide the necessary interaction between the individual complexes that leads to the sharp LS to HS transition.

The calculated normal coordinates allow a detailed discussion of the experimental IR and Raman spectra. The good correlation between experimental and calculated wavenumbers justifies the attempt to determine the entropy change associated with the molecular vibrations on the basis of the theoretical spectra. The effect of inter-molecular interaction manifests itself clearly in the small shifts of several bands associated with pyridine-localized and N≡CS stretching motions, when the sample approaches the conversion temperature.

Our estimation of the vibration-correlated entropy change yields $\Delta S_{vib} \sim 40.3$ J/(mol·K). The change in spin distribution contributes, in addition, $\Delta S_{el} = 14$ J/(mol·K). Both contributions together are larger than the average value determined for a series of spin-crossover compounds. It

would therefore be interesting to have an experimental value for the total entropy change, ΔS_{tot}, to find out whether the compound investigated exhibits an unusually large entropic driving force and to speculate about its origin.

Acknowledgements

REFERENCES

1. Cambi L, Cagnasso A. *Atti Accad. Naz. Lincei* 1931; **13**: 809.
2. Cambi L, Szego L. *Ber. Dtsch. Chem. Ges.* 1931; **64**: 259.
3. Gütlich P, Hauser A, Spiering H. *Angew. Chem.* 1994; **106**: 2109.
4. Gütlich P, Goodwin HA. *Topics in Current Chemistry*, vol. 235. Springer: Berlin, 2004; 268.
5. Bousseksou A, Molnar G, Matouzenko GS. *Eur. J. Inorg. Chem.* 2004; **22**: 4353.
6. Spiering H, Boukheddaden K, Linares J, Varret F. *Phys. Rev. B: Condens. Matter Mater. Phys.* 2004; **70**: 184 106/1.
7. Achim C. *J. Am. Chem. Soc.* 2005; **127**: 1061.
8. Sorai M, Seki S. *J. Phys. Chem. Solids* 1974; **35**: 355.
9. Sorai M. *Topics in Current Chemistry*, vol. 235. Springer: Berlin, 2004; 253.
10. Tuchagues J-P, Bousseksou A, Molnar G, McGarvey JJ, Varret F. *Topics in Current Chemistry*, vol. 235. Springer: Berlin, 2004; 85.
11. Linert W, Grunert MC, Koudriavtsev AB. *Topics in Current Chemistry*, vol. 235. Springer: Berlin, 2004; 105.
12. Bousseksou A, McGarvey JJ, Varret F, Real JA, Tuchagues J-P, Dennis C, Boillot ML. *Chem. Phys. Lett.* 2000; **318**: 409.
13. Brehm G, Reiher M, Schneider S. *J. Phys. Chem. A* 2002; **106**: 12 024.
14. Reiher M, Brehm G, Schneider S. *J. Phys. Chem. A* 2004; **108**: 734.
15. Leibold M. Synthese und charakterisierung von kupfer-, Eisen – und Zinkkomplexen mit tripodalen Liganden, Master Thesis, Universität Erlangen-Nürnberg, 2000.
16. Leibold M, Heinemann F, Hampel F, Renz F, Toftlund H, Brehm G, Schneider S, Reiher M, Schindler S Manuscript in preparation for submission to JACS.
17. Matouzenko GS, Bousseksou A, Lecocq S, van Koningsbruggen PJ, Perrin M, Kahn O, Collet A. *Inorg. Chem.* 1997; **36**: 2975.
18. Højland F, Toftlund H, Yde-Anderen S. *Acta Chem. Scand.* 1983; **A37**: 251.
19. Ahlrichs R, Bär M, Häser M, Horn C, Kölmel C. *Chem. Phys. Lett.* 1989; **162**: 165.
20. Becke AD. *Phys. Rev., A* 1988; **38**: 3098.
21. Perdew JP. *Phys. Rev., B* 1986; **33**: 8822.
22. Eichkorn K, Treutler O, Öhm H, Häser M, Ahlrichs R. *Chem. Phys. Lett.* 1995; **240**: 283.
23. Eichkorn K, Weigend F, Treutler O, Ahlrichs R. *Theor. Chem. Acc.* 1997; **97**: 119.
24. Schäfer A, Huber C, Ahlrichs RJ. *J. Chem. Phys.* 1994; **100**: 5829.
25. Neugebauer J, Reiher M, Kind C, Hess BA. *J. Comput. Chem.* 2002; **23**: 895.
26. Reiher M, Neugebauer J, Hess BA. *Z. Phys. Chem.* 2003; **217**: 91.
27. Neugebauer J, Hess BA. *J. Chem. Phys.* 2003; **118**: 7215.
28. Reiher M, Salomon O, Hess BA. *Theor. Chem. Acc.* 2001; **107**: 48.
29. Reiher M. *Inorg. Chem.* 2002; **41**: 6928.
30. Schaftenaar G, Noordik JH. Molden: a pre- and post-processing program for molecular and electronic Structures. *J. comput. Aided Mol. Design.* **14**: 2000; 123; www.cmbi.ru.nl/molden/molden.html.
31. Burnett MN, Johnson CK. *ORTEP III*, www.ornl.gov/sci/ortep/ortep.html [Jan 31, 2000].

32. Wilson EB, Decius JC, Cross PC *Molecular Vibration*. McGraw-Hill: New York, 1955.
33. Varsanyi G. *Vibrational Spectra of Benzene Derivatives*. Academic Press: New York, London, 1969.
34. Takemoto JH, Hutchinson B. *Inorg. Chem.* 1973; **12**: 705.
35. Wu D-Y, Ren B, Jiang Y-X, Xu X, Tian Z-Q. *J. Phys. Chem. A* 2000; **106**: 9042.
36. Osaki T, Yoshikawa T, Satoh Y, Shimada R. *J. Raman Spectrosc.* 2005; **36**: 199.
37. Paulsen H, Winkler H, Trautwein AX, Grünsteudel H, Rusanov V, Toftlund H. *Phys. Rev., B* 1999; **59**: 975.
38. Paulsen H, Benda R, Herta C, Schünemann V, Chumakov AI, Duelund L, Winkler H, Toftlund H, Trautwein AX. *Phys. Rev. Lett.* 2001; **86**: 1351.
39. Scott AP, Radom L. *J. Phys. Chem.* 1996; **100**: 16 502.